Manuscript ID: egusphere-2026-2297

Reviewer 1's responses are on pages 1–13, and Reviewer 2's on pages 14–18.

Responses to Reviewer 1

We would like to thank the Editor and the Reviewer for their careful reading of the manuscript and for the constructive comments and suggestions. We have revised the manuscript accordingly and provide point-by-point responses below. Our responses are shown in blue, the corresponding changes made in the revised manuscript are shown in red, and the Reviewer's comments are shown in black.

Brief Summary:

The Reviewer recognizes the relevance and novelty of the global deep-atmosphere GMCORE formulation on a regular latitude–longitude grid, while requesting additional details on the numerical methods, standard validation tests, computational performance, and interpretation of the tropical-cyclone results.

Response: Thank you very much for the careful reading, the positive assessment of the novelty of the global deep-atmosphere GMCORE formulation, and the detailed suggestions. We understood the central concern to be that the original manuscript did not provide sufficient numerical detail and validation context for readers to assess the implementation with confidence. Accordingly, we have tried to make the revision explicit about what is implemented, how it is discretized, what has been tested, and where our physical interpretation remains tentative. We respond to each point below and have avoided adding claims that are not directly supported by the present experiments.

Line numbers cited below refer to the revised manuscript supplied with this response after accepting the tracked changes.

Major issues

1. Relevant literature. The introduction lacks in addressing relevant literature. Below is a list of suggestions:

1. Add the publication of Becker and Vadas (2020, https://doi.org/10.1029/2020JA028034) as it comprises several similarities to the present study and poses a substantial achievement in the field of upper-atmosphere modeling.

2. The paper puts some focus on the non-traditional component of the Coriolis force that is usually neglected. Adding the publication of Chew et al. (2022, https://doi.org/doi:10.1017/jfm.2023.474) would help to sharpen the discussion on the relevance of this term.

Response: Thank you for these helpful literature suggestions. We agree that they strengthen two complementary parts of the motivation. Becker and Vadas (2020) places the present work in the context of whole-atmosphere modelling and explicitly resolved gravity-wave propagation into the thermosphere, while the paper suggested by the Reviewer on the nontraditional Coriolis acceleration sharpens the physical motivation for retaining the full Coriolis vector. We have added both references and cite the latter using its final publication year, Chew et al. (2023).

Revised manuscript text [Lines 26–28 and 50–52]: "The HIAMCM models (Becker and Vadas, 2020), with a nonhydrostatic correction, achieves the explicit simulation of gravity waves reaching the thermosphere." "Recent studies have further shown that retaining the full Coriolis acceleration can influence the stability characteristics of atmospheric wave modes (Chew et al., 2023)."

2. Numerical discretization and model formulation. Section 2 would greatly benefit from adding more detail to the discretization strategy. In particular, please add

2.1 Vertical grid and vertical domain. A description of the vertical grid, i. e., the effective spatial distribution of vertical levels and the vertical extent of the physical domain;

Response: Thank you for this suggestion. We agree that the original description was too abstract. The revised manuscript now separates the general definition of the hybrid dry-mass vertical coordinate from the concrete vertical grid used in the experiments. Section 2.2 defines the hybrid

coefficients and model interfaces, Sect. 2.3 states the Lorenz vertical staggering, and Sect. 3 gives the actual 30-level CAM grid and model-top setting used in the simulations.

Revised manuscript text [Lines 137–140, 166–172, and 366–370]: "The coefficients η_A and η_B prescribe a set of hybrid coordinate defined at the model interfaces. The uppermost interface defines the model top, whereas the lowest interface follows the lower boundary. The specific vertical resolution and model-top setting used in each experiment are given in Sect. 3." "GMCORE uses an Arakawa C-grid staggering in the horizontal and a Lorenz staggering in the vertical ... The vertical velocity w and vertical coordinate velocity $\dot{\eta}$ are defined at the half levels." "The simulations use the 30-level vertical grid adopted from CAM, with the model top located at 2.255 hPa, corresponding to an approximate geometric height of 30 km."

2.2 Model-top sponge layer. A comment on whether a sponge layer at the model top is necessary to stabilizethe numerics;

Response: Thank you for raising this question. It is useful for distinguishing an upper-boundary numerical treatment from the deep-atmosphere formulation itself. GMCORE includes an optional upper-level Rayleigh damping of vertical velocity. It is not activated in either idealized experiment presented here because the model tops are comparatively low and the integrations remain stable without a sponge layer. We now state this explicitly and clarify the intended role of this option in future high-top applications.

Revised manuscript text [Lines 355–358]: "GMCORE also provides an optional upper-level Rayleigh damping of vertical velocity. This damping is not activated in the two idealized cases presented here; with their comparatively low model tops, both cases remain numerically stable without a sponge layer. For future high-top applications, the same damping option can be used as an upper-boundary treatment to attenuate upward-propagating disturbances and reduce artificial reflection, rather than as a correction to the deep-atmosphere equations themselves."

2.3 Orography and geoid deformation. A comment on the treatment of orography and the geoid deformation from the perfect sphere;

Response: Thank you for raising this point. We have made the geometric assumptions explicit. The present implementation uses a spherical reference planet. Orography can enter through the lower-boundary surface geopotential and the terrain-following coordinate, whereas the idealized experiments in this manuscript use zero orography. Departures of the geoid from a perfect sphere, including oblateness, are not represented in the present version.

Revised manuscript text [Lines 156–158]: "The present deep-atmosphere geometry uses a spherical reference planet. Orography can enter through the lower-boundary surface geopotential and the terrain-following η coordinate, but the idealized experiments reported here use zero orography. Deviations of the geoid from a perfect sphere, such as oblateness, are not represented in the present version."

2.4 Motivation for the regular latitude–longitude grid. A motivational comment on why you chose the discretization based on a regular lat-lon grid. Since the majority of the community agreed on circumventing the pole-problem by taking more advanced gridding strategies into account, a motivation would be suitable as to why the grid type presented here is relevant. Please address advantages and potential pitfalls;

Response: Thank you for raising this important point. We agree that quasi-uniform grids are attractive because they avoid the severe polar convergence of a regular latitude–longitude mesh. Our intention is not to argue that the regular latitude–longitude grid is generally superior. Rather, GMCORE retains it as a practical design choice because of its orthogonality, the direct physical meaning of the zonal and meridional directions, and consistency with the existing GMCORE numerical structure. We have also added context that the regular latitude–longitude grid remains an established global-grid option (Staniforth and Thuburn, 2012) and continues to be developed, for example by Lima (2024). We now state these advantages together with the principal drawback—the shrinking zonal grid spacing and the associated polar CFL restriction—and describe the adaptive Gaussian filter as a practical mitigation. With the same motivation of reducing the polar limitation, our group is also attempting to construct an SCVT-based hexagonal-grid framework; this is an ongoing development and is outside the scope of the present manuscript.

Revised manuscript text [Lines 160–165 and 313–343]: "The regular latitude–longitude grid remains widely used in several established atmospheric models (Williamson, 2007; Staniforth and Thuburn, 2012) and is still under continuous development (Lima, 2024). Its orthogonal geometry aligns the coordinate directions with the zonal and meridional flow components, facilitating the formulation of fluxes and differential operators. GMCORE retains this grid structure as a practical choice that is consistent with its existing numerical framework. However, the convergence of meridians toward the poles leads to increasingly small zonal grid spacing and restrictive stability constraints, requiring the polar filtering treatment described in Sect. 2.5." Sect. 2.5 then defines the latitude-dependent Gaussian filter and documents the wider high-latitude communication halo, including the representative 1° half-width of about 90 grid points.

2.5 Horizontal discretization. Please add details on the horizontal discretization strategy.

Response: Thank you for this request. We agree that this part of the original manuscript was too brief. Section 2.3 has therefore been substantially expanded. The revised description now includes the C-grid/Lorenz staggering, radius-dependent cell areas and edge lengths, finite-volume divergence and gradient operators, circulation-based relative vorticity and layer-mass PV, the third-order upwind PV reconstruction and transverse flux mapping, kinetic-energy gradient, Simmons–Burridge vertical advection, and the perturbation-form pressure-gradient force. We also state where the local-radius metric factors are evaluated on the staggered grid so that the deep-atmosphere modifications can be followed at the discrete level.

Revised manuscript text [Lines 160–260]: Sect. 2.3 now introduces the regular latitude–longitude-grid motivation, C-grid/Lorenz staggering, cell/edge/vertex notation, radius-dependent discrete geometry, finite-volume divergence and gradient, vorticity/PV and rotational tendency, kinetic-energy gradient, vertical momentum advection, pressure-gradient force, and tracer transport. In particular, Lines 189–194 state: "Let a be the reference planetary radius and r_c, r_e, and r_v the local radial distances at cell, edge, and vertex locations. A superscript (a) denotes the corresponding horizontal geometry on the reference sphere. The deep-atmosphere metric is therefore introduced directly through the local lengths and areas ... The shallow-atmosphere form is recovered when $r_c = r_e = r_v = a$. Vertical transport uses the analogous shell-area factor $(r/a)^2$ at layer interfaces."

2.6 Time stepping. Please add more details on the time-stepping strategy, e. g., at the example of one prototypical equation.

Response: Thank you for this request. We understood it as asking for the actual update sequence rather than only a statement that the method is semi-implicit. We have therefore added a prototype prognostic equation and the modified three-stage Runge–Kutta update, followed by the explicit/implicit split used at each stage. We also added a short transition explaining that the vertical momentum and geopotential equations form the core of the vertically coupled fast-wave subsystem. The revised text then shows how the vertical pressure-gradient/geopotential coupling leads to a one-dimensional tridiagonal system for vertical velocity in each column and how the remaining implicit increments are recovered by back-substitution.

Revised manuscript text [Lines 265–311]: "After the spatial discretization described in Sect. 2.3, the governing equations can be written in the following prototype form ... GMCORE advances Eq. (33) using a modified three-stage Runge–Kutta scheme (Wicker and Skamarock, 2002)." The revised text further states that "Each Runge–Kutta stage can be regarded as a forward-in-time update over the corresponding stage interval," identifies the vertically coupled nonhydrostatic subsystem formed by the vertical momentum and geopotential equations, and then derives the columnwise tri-diagonal vertical-velocity system and back-substitution procedure.

3. Test-case configuration. In section 3, generally more information is needed on the test cases that is specific to the presented model. For all presented test cases, if not already included, please add information on.

3.1 the vertical resolution.

Response: Thank you for requesting the model-specific vertical resolution. We have added it explicitly. The baroclinic-wave simulations use the 30-level vertical grid adopted from CAM, and the tropical-cyclone simulations use the same vertical grid.

Revised manuscript text [Lines 366–367 and 443]: “The simulations use the 30-level vertical grid adopted from CAM ...” “We follow the standard setup of Reed and Jablonowski (2011) and run this case at a horizontal resolution of 0.25° and 0.125° for 10 days with the same vertical grid as the baroclinic-wave.”

3.2 the vertical extent of the simulation.

Response: Thank you for this request. It is now stated together with the vertical resolution. For the baroclinic-wave experiment, the model top is 2.255 hPa, corresponding to an approximate geometric height of 30 km. The tropical-cyclone experiment uses the same vertical grid.

Revised manuscript text [Lines 366–367 and 443]: “The simulations use the 30-level vertical grid adopted from CAM, with the model top located at 2.255 hPa, corresponding to an approximate geometric height of 30 km.” The tropical-cyclone section likewise notes “the low model top (about 30 km)” and states that the same vertical grid as the baroclinic-wave is used.

3.3 the horizontal resolution.

Response: Thank you for this request. They are now stated explicitly. The baroclinic-wave experiment uses a 1° (360×180) regular latitude–longitude grid. The tropical-cyclone experiments are performed at 0.25° and 0.125°.

Revised manuscript text [Lines 367–368 and 442–443]: “The horizontal resolution is 1°, corresponding to a 360×180 regular latitude–longitude grid.” “We follow the standard setup of Reed and Jablonowski (2011) and run this case at a horizontal resolution of 0.25° and 0.125° for 10 days ...”

3.4 HPC configuration (number of nodes and cores, walltime).

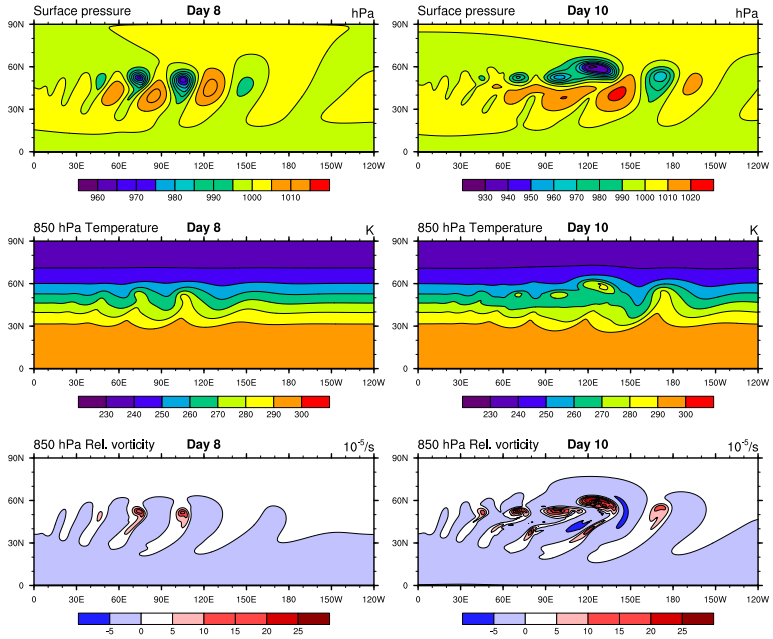
Response: Thank you for this request. We have added representative computational information for both test cases. The 1° baroclinic-wave experiment is decomposed in latitude and was run on 2 compute nodes with 120 CPU cores in total; the reported integration required approximately 5 min of wall-clock time. For the tropical-cyclone experiments, the revised manuscript reports 480 cores and a walltime around 120 min at 0.25°, and 600 cores and a walltime around 900 min at 0.125°.

Revised manuscript text [Lines 368–370 and 442–444]: “The domain is decomposed along the latitude direction for parallel computation. The simulations were performed using 2 compute nodes with 120 CPU cores in total, and the wall-clock time for the integration reported here was approximately 5 min.” “The 0.25° simulations were performed using 480 CPU cores with a walltime around 120 minutes, whereas the 0.125° simulations used 600 CPU cores with a walltime around 900 minutes.”

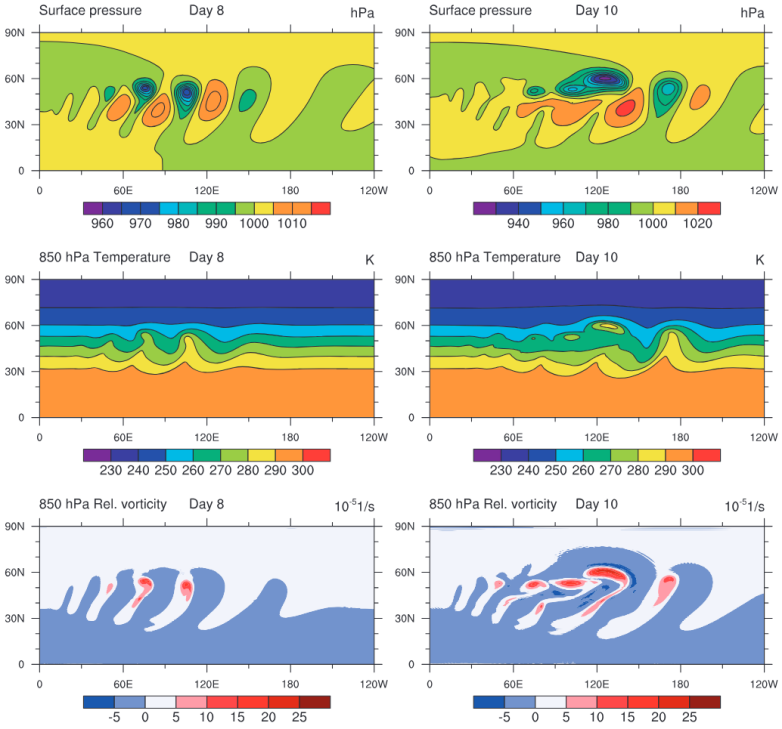
4. Comparison with established models. Please address the question on how the model compares to established models. If feasible, add a comparison.

Response: Thank you for this suggestion. We interpret this point as asking whether the implementation reproduces the characteristic behaviour reported for established deep-atmosphere dynamical cores, rather than requiring a pointwise code-to-code comparison across different grids, diffusion choices, time integration, and initialization. We have therefore strengthened the literature-based benchmark comparison. The standard-Earth baroclinic-wave evolution is compared with published results from Ullrich et al. (2014), ENDGame (Wood et al., 2014), UA-ICON (Borchert et al., 2019), MPAS-A (Skamarock et al., 2021), NUMA (Kelly et al., 2026), and CliMA (Yatunin et al., 2026). In the X20 experiment, GMCORE reproduces the characteristic stronger and more rapidly developing deep-atmosphere solution reported in the literature.

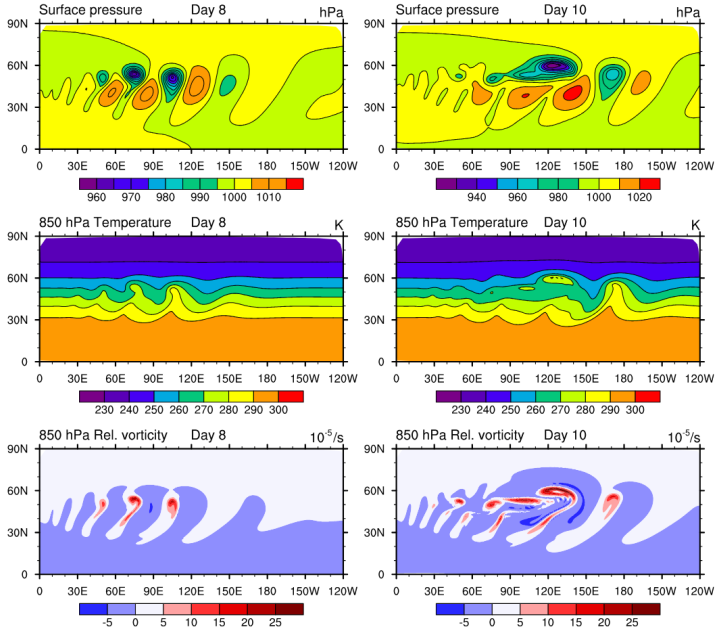
GMCORE:



MCORE:



MPAS

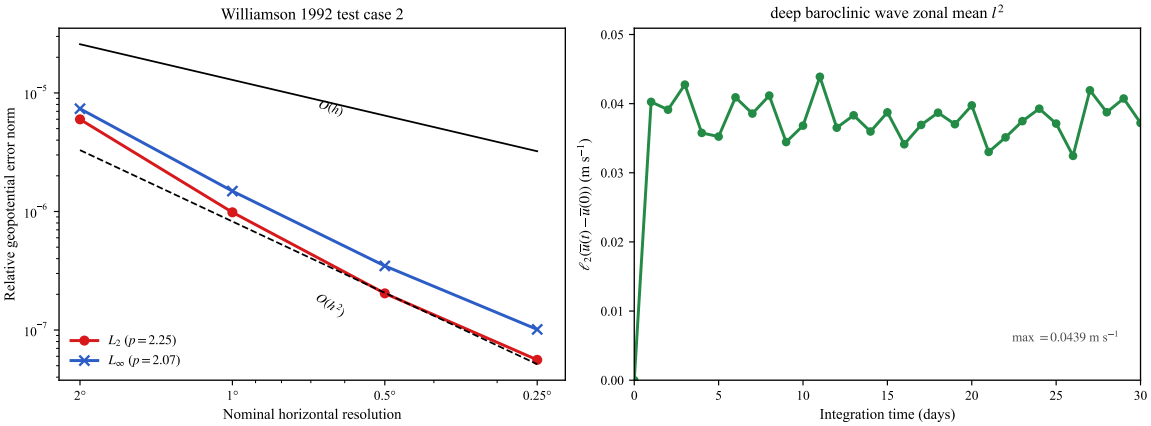


Revised manuscript text [Lines 392–396 and 418–426]: "Overall, the simulated fields are consistent with the standard behaviour reported in previous model intercomparisons of this test case (Ullrich et al., 2014; Wood et al., 2014; Borchert et al., 2019; Skamarock et al., 2021; Kelly et al., 2026; Yatunin et al., 2026) ..." In the X20 experiment, the manuscript states that the deep-atmosphere solution shows more rapid amplification and stronger cyclonic development and that this behaviour is consistent with Ullrich et al. (2014).

5. Convergence, stability, performance, and CFL. For the sake of assessing the usability of the model, for at least one of the presented test cases, please add.

5.1 A convergence study demonstrating the consistency and stability of the model;

Response: Thank you for this request. We agree that both are important for assessing the consistency of the numerical implementation. Because the basic flow in the baroclinic-wave test is geostrophically balanced, we use the steady barotropic geostrophic-flow test of Williamson et al. (1992), for which an analytical solution is available, to examine horizontal convergence. The test is integrated at 2°, 1°, 0.5°, and 0.25°, with time steps of 600, 300, 150, and 75 s. The fitted relative-geopotential convergence orders are 2.25 for L_2 and 2.07 for L_∞, indicating near-second-order convergence. As a complementary stability check, following Jablonowski and Williamson (2006), we integrate the unperturbed standard-Earth baroclinic-wave basic state; the zonal-mean wind-deviation norm remains below 0.044 m s−1 throughout the 30-day integration.

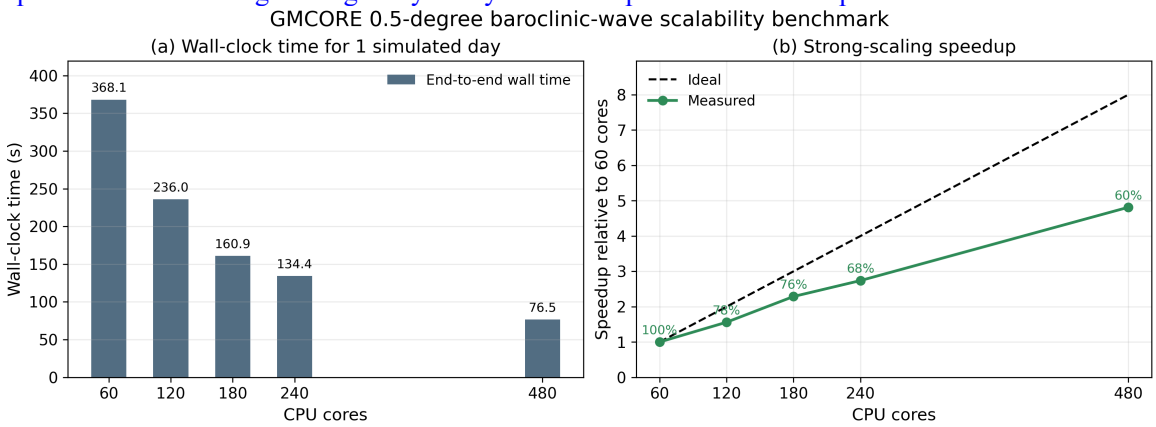


Revised manuscript text [Lines 383–388]: "Steady geostrophic flow is integrated for 5 days at nominal horizontal resolutions of 2°, 1°, 0.5°, and 0.25°, with time steps of 600, 300, 150, and 75 s, respectively. The fitted convergence orders of the relative geopotential errors are 2.25 for L2 and 2.07 for L∞, indicating near-second-order convergence ... On the 1° grid, the norm remains below 0.044 m/s throughout the 30-day integration, indicating stable preservation of the balanced basic state."

5.2 A performance benchmark indicating the scalability of the model.

Response: Thank you for this request. We have added the actual computational configurations and wall-clock information used for the experiments. The current latitude-band decomposition is still affected by the wider halo exchanges required by the adaptive polar Gaussian filter, and this communication pattern has not yet been fully optimized for a formal large-core strong-scaling assessment. We therefore report the representative computational cost used in the present experiments and regard a systematic scalability study as part of our ongoing parallel-optimization work.

In addition, we conducted a benchmark experiment for the 0.5° deep-atmosphere baroclinic-wave case and measured the wall-clock time over several CPU-core counts, as shown below. The test provides a practical indication of the present parallel behaviour, while a more systematic HPC optimization and strong-scaling study is beyond the scope of this manuscript.



Revised manuscript text [Lines 340–343, 368–370, and 442–444]: Sect. 2.5 states that the wider communication halo is required only for the variables to which the filter is applied and that, at 1° resolution, the half-width usually reaches about 90 grid points near the poles. Sect. 3 reports the 2-node/120-core baroclinic-wave configuration with an approximately 5 min wall-clock time, and the tropical-cyclone configurations of 480 cores/approximately 120 min at 0.25° and 600 cores/approximately 900 min at 0.125°.

5.3 A comment on the typically achieved CFL numbers for you test cases.

Response: Thank you for this request. We have added this information for the baroclinic-wave experiment. With a 300 s time step, the gravity-wave CFL number is approximately 0.27 near the equator, 0.39 at midlatitudes, and 0.64 at 60°. It exceeds unity poleward of about 70° because of the shrinking zonal grid spacing, where the latitude-dependent Gaussian filter is applied. The vertically propagating acoustic terms are treated semi-implicitly to relax their CFL constraint.

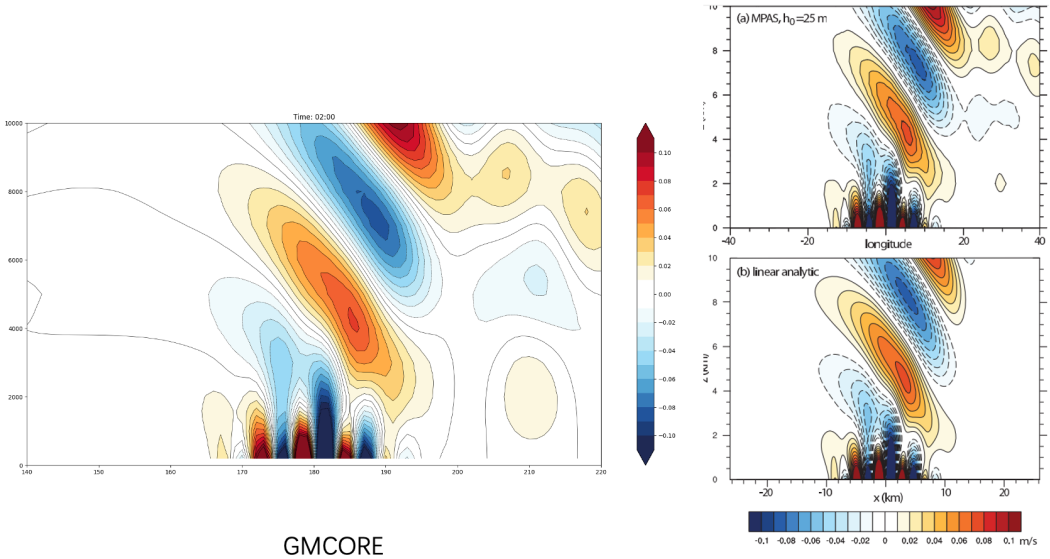
Revised manuscript text [Lines 401–403]: "With a timestep of 300 s, the gravity-wave CFL number is approximately 0.27 near the equator, 0.39 at midlatitudes, and 0.64 at 60°. It exceeds unity poleward of about 70° because of the reduced zonal grid spacing, where a latitude-dependent Gaussian filter is applied. Vertical acoustic terms are treated semi-implicitly to relax their CFL constraint."

6. Gravity-wave representation. Since you are achieving the horizontal resolution necessary to explicitly resolve sub-stantial parts of the gravity wave spectrum, a test case showcasing the representation of gravity waves would be appropriate.

Response: Thank you for this suggestion. At present, GMCORE has implemented several nonhydrostatic orographic gravity-wave tests, including the Klemp et al. (2015) test, the

DCMIP2025 mountain-wave-breaking test (not yet formally published), and the Kelly et al. (2026) test. For the Kelly et al. (2026) case, after communication we have not yet obtained the temperature-profile and surface-pressure data needed to reproduce the published initialization completely, and our present result therefore differs clearly from that reported in their paper. The MPAS gravity-wave tests we considered are mainly two-dimensional, and we have not attempted them in the present work. We are also trying to formulate a new deep-atmosphere gravity-wave test based on the profile of Staniforth and White (2008), but with our present progress it is difficult to include a sufficiently mature result in this revision. We hope the Reviewer will agree that gravity-wave propagation in a genuinely high-top configuration deserves a dedicated follow-up study.

Klemp et al. (2015) Fig. 2

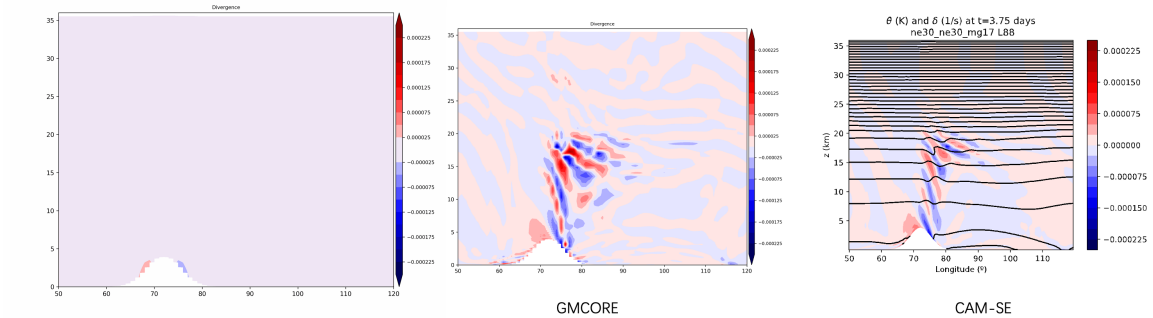


GMCORE

Klemp et al.(2015)

West-east vertical cross section of vertical velocity along the ridge centerline at 2h

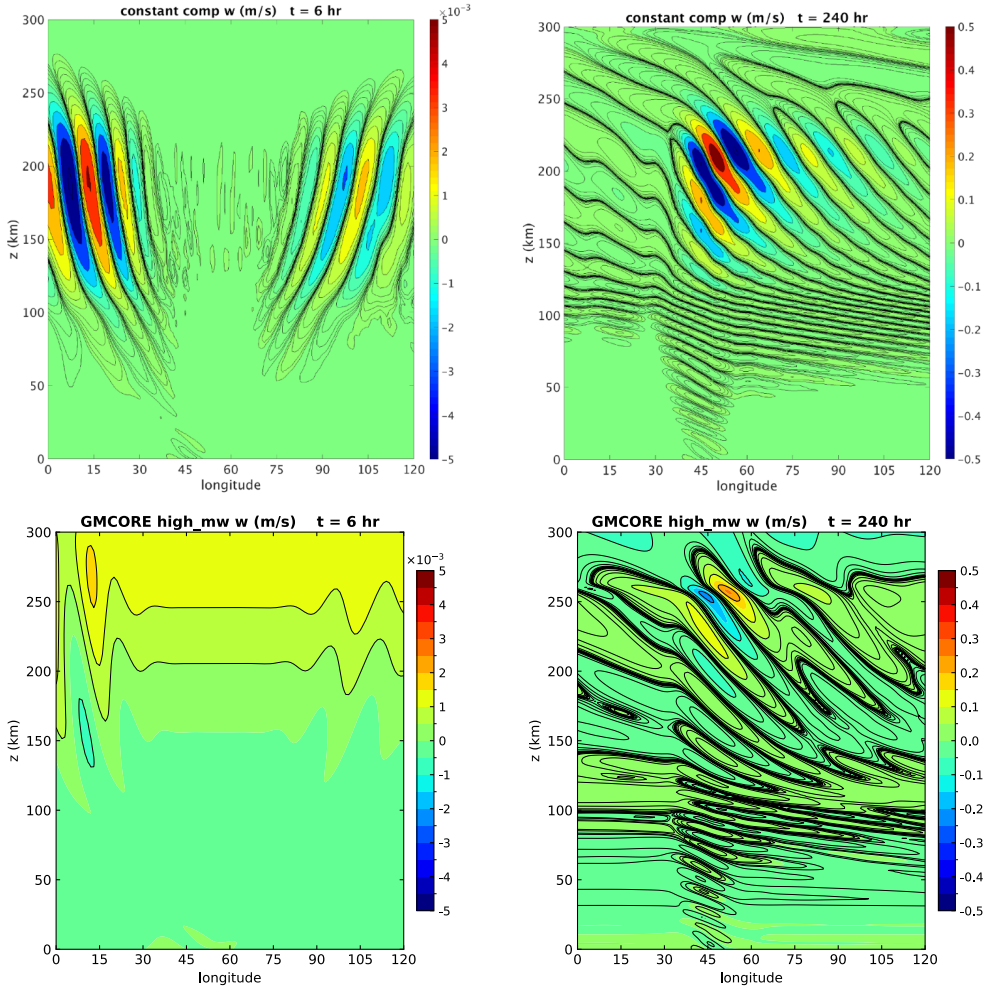
DCMIP2025 test case 1: Mountain-triggered breaking gravity waves:



GMCORE CAM-SE

Meridional cross section of horizontal divergence at 35°N ($t = 3.75\text{day},\ \text{res}\sim1°, \Delta z = 800m$)

Kelly et al. (2026): Fig. 10



Longitude-altitude cross sections along the equator of vertical velocity w (res~1° , gmcore $\Delta z = 1km$)

Revised manuscript text [Lines 355–358 and 568–570]: No additional gravity-wave benchmark is claimed in the revised manuscript. Sect. 2.5 states that the optional upper-level Rayleigh damping can be used in future high-top applications to attenuate upward-propagating disturbances and reduce artificial reflection. The Conclusions state: "Future work will therefore focus on extending these diagnostics, raising the model top together with appropriate physical parameterizations, and further evaluating gravity-wave and upper-atmosphere dynamics."

Localized comments:

L156–157. The statement "This staggering optimally represents inertia-gravity wave dispersion characteristics and suppresses computational mode" should be justified with a reference.Also give a reference to the advection scheme SWIFT.

Response: Thank you for pointing this out. We have revised the C-grid sentence to avoid the overly absolute wording "optimally represents" and have added supporting references. We have also added the formal SWIFT reference and retained Lin and Rood (1996) for the broader FFSL transport context. In the revised numerical description, PPM is used for the SWIFT reconstruction.

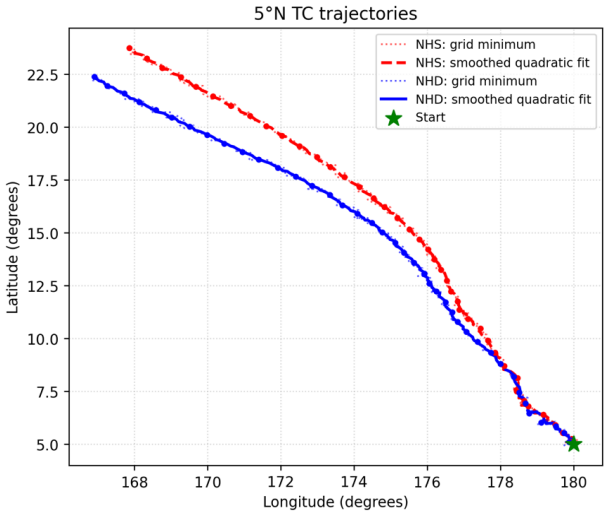
Revised manuscript text [Lines 166–172 and 257–260]: "GMCORE uses an Arakawa C-grid staggering in the horizontal and a Lorenz staggering in the vertical ... The Arakawa C-grid is well suited for representing geostrophic adjustment and inertia–gravity waves, while the Lorenz vertical staggering has a relatively simple structure and facilitates conservative discretization (Arakawa and Lamb, 1977; Adcroft et al., 1997; Simmons and Burridge, 1981)." "Tracer advection is handled by the SWIFT scheme (Bendall and Kent, 2025), which is derived from the

FFSL formulation (Lin and Rood, 1996) with specific modifications to preserve monotonicity in two-dimensional transport and relies on PPM for the spatial reconstruction of tracers."

Figure 3->5. The asymmetry of the storm can affect the ability of "naive" methods to identify the storm center. Therefore, please give details on how the storm center is computed.

Response: Thank you for this request. We agree that the definition should be documented because the later storm-centered diagnostics are sensitive to recentering. In the revised manuscript, the trajectory figure is now Fig. 5. For the trajectory itself, the storm center is diagnosed directly from the grid-point minimum of surface pressure at each output time. For the storm-relative diagnostics in Figs. 6 and 7, a smoother sub-grid center is used: the center is first located near the storm position at the previous output, a two-dimensional quadratic surface is fitted to the surrounding 5×5 surface-pressure grid points, and the local minimum of the fitted surface is used as the sub-grid center. We do not claim an additional center-definition sensitivity experiment because such a comparison was not part of the present analysis.

We also plot the two methods of storm-centered diagnostics.



Revised manuscript text [Lines 460–461 and 476–478]: The Fig. 5 caption states: "Storm centers are diagnosed directly from the grid-point minimum of surface pressure." The Fig. 6 caption states: "The center is first identified within a neighbourhood of the storm position at the preceding output time. A two-dimensional quadratic surface is then fitted to the surrounding 5×5 grid points, and the local minimum of the fitted surface is used as the sub-grid storm center."

Section 3.2.1. You traced-back the observed drift of the deep-atmosphere simulation compared to the shallow approximation to the structural differences without further contextualization of the underlying mechanisms. There is a substantial amount of literature in the context of TC asymmetries and their effect on the storm track evolution. I recommend consulting to the work of Polvani, Reasor, Montgomery, Nolan, Schecter, Paeschke, and Doerffel. Please add a short discussion.

Response: Thank you for directing us to this literature. We understood the intent to be more than simply adding citations: the deep–shallow drift should be discussed in the established language of asymmetric-vortex dynamics, while the mechanistic claim should remain commensurate with the diagnostics available here. We have therefore added a short discussion linking the diagnosed NCT-related dipole to an azimuthal-wavenumber-one structure. For an approximately axisymmetric eyewall updraft, the storm-centered polar-coordinate relation gives $\frac{\partial w_0}{\partial y} = \frac{dw_0}{dr}\sin\theta$, so the NCT contribution proportional to $2\Omega\cos\phi$ naturally projects onto an $m = 1$ tendency. We then connect this structure with displacement/tilt, vortex-Rossby-wave adjustment, precession, alignment, and centerline-motion studies, including Dörffel et al. (2021). We state that this is a dynamically consistent interpretation rather than a closed causal proof. The specific effect of the

$2\Omega \cos \phi$ terms on tropical-cyclone motion and asymmetric vortex evolution will remain a subject of our continuing research.

Revised manuscript text [Lines 513–530 and 531–537]: "For this reason, the mechanism discussed above should be taken as an interpretation of the present results rather than as a complete dynamical proof." The revised discussion then places the NCT-induced wavenumber-one tendency in the context of Polvani (1991), Reasor and Montgomery (2001), Nolan et al. (2001), Schecter et al. (2002), Päschke et al. (2012), and Dörffel et al. (2021), and states that determining how the forcing is partitioned among vortex-Rossby-wave adjustment, trochoidal displacement, and three-dimensional tilt or centerline precession is a direction for further investigation. The subsection concludes that more complete angular-momentum, potential-vorticity, and asymmetric-flow budgets are required to quantify the mechanism.

Minor issues

1. L27. You refer to Borchert et al. (2019) as a reference to the ICON model development. While it is the reference publication for the upper-atmosphere extension of ICON (UA-ICON), the reader may be benefit from a reference to the technical description of the base model ICON, presented by Zängl et al. (2015)).

Response: Thank you for this citation suggestion. We have added Zängl et al. (2015) alongside the UA-ICON reference so that the base ICON dynamical-core formulation and its upper-atmosphere extension are cited separately.

Revised manuscript text [Lines 27–31]: The model list now includes "... MPAS-A (Skamarock et al., 2021), ICON (Zängl et al., 2015; Borchert et al., 2019), NUMA (Kelly et al., 2026) and CliMA (Yatunin et al., 2026) ..."

2. L51. The plural noun "researches" is unusal. It could be replaced by studies.

Response: Thank you for noting this wording issue. We have replaced the unusual plural noun "researches" with "studies" as suggested.

Revised manuscript text [Lines 54–57]: "GMCORE is a fully compressible nonhydrostatic dycore formulated on a latitude–longitude C grid with a dry terrain-following mass-based coordinate (Li et al., 2020; Li and Dong, 2024), and has been applied to Mars climate simulation studies (Dong et al., 2023; Liu et al., 2026)."

3. Equations (1–7). Here you use the governing equations using the Lamb transformation as presented in Gassmann and Herzog (2008, https://doi.org/10.1002/qj.297). This reference should be given.

Response: Thank you for this reference suggestion. We have added Gassmann and Herzog (2008) and clarified that the governing equations are written in the corresponding Lamb-transformed/vector-invariant form.

Revised manuscript text [Lines 77–80]: "Following the vector-invariant formulation based on the Lamb transformation (Gassmann and Herzog, 2008), together with the deep-atmosphere formulations of Wood and Staniforth (2003), Borchert et al. (2019), and Skamarock et al. (2021), GMCORE solves the fully compressible, nonhydrostatic deep-atmosphere equations in a dry terrain-following mass-based coordinate in vector-invariant form."

4. L84. The term "horizontal operator" is unprecise. You might use "horizontal differential operator".

Response: Thank you for this correction. We have replaced "horizontal operator" with "horizontal differential operator" as suggested.

Revised manuscript text [Lines 90–94]: "Here $V = (ui, vj)$ is the wind vector, $\dot{\eta}$ is the vertical coordinate velocity, ∇_η^d is the deep-atmosphere horizontal differential operator ..."

5. L115. You use the term "local edge modification" without introducing its meaning. Since (I assume) it is specific to your discretization approach, a brief explanation would be appropriate. Refer also to the major comment regarding the presentation of the discretization.

Response: Thank you for asking us to clarify this term. We have replaced the undefined shorthand with an explicit description of the radius-dependent scaling of edge length and face fluxes, and we now define where the metric factor is evaluated on the staggered grid.

Revised manuscript text [Lines 121–127]: "The vertical transport operator requires a different geometric correction ... whereas the horizontal transport uses a local edge modification, i.e., the radius-dependent scaling of each horizontal grid-edge length by the local factor (r/a), together with the deep-atmosphere horizontal divergence operator on the staggered grid."

6. L124. For the description of the vertical coordinate, you use the terms $\rho r^2 \frac{\partial r}{\partial s}$ and $\rho a^2 \frac{\partial r}{\partial s}$ without introducing the meaning of s. Please add this context or adjust the symbol.

Response: Thank you for pointing this out. We now define s explicitly as the generalized vertical coordinate used in the Wood and Staniforth (2003) derivation and distinguish it from the terrain-following coordinate η used in the GMCORE implementation.

Revised manuscript text [Lines 130–140]: "As demonstrated by Wood and Staniforth (2003), a mass-based vertical coordinate requires adjustment for the deep-atmosphere. They denoted s as the generalized vertical coordinate ... We use the dry mass π to substitute the generalized coordinate s and introduce terrain-following coordinate η (Kasahara, 1974; Simmons and Burridge, 1981)."

7. L133. The use of ∂ as a differential is rather unusual. It should be replaced by d.

Response: Thank you for this correction. We have used d rather than ∂ for the ordinary differential as suggested.

Revised manuscript text [Lines 141–149]: The hydrostatic derivation now uses ordinary differential notation; the manuscript states: "Recognizing the exact differential form $r^2 dr = (1/3)d(r^3)$, this relation can be analytically integrated from the planetary surface ..."

8. Equation (20). Please introduce the variable γ.

Response: Thank you for asking us to define γ. We have introduced it immediately after Eq. (37) and defined it as the ratio of the specific heats at constant pressure and constant volume.

Revised manuscript text [Lines 294–299]: "At full levels, the temporal increment of pressure $p^\tau - p^*$ is diagnostically linked to vertical increment of $\delta\varphi$ and the thermodynamic properties through the linearized equation of state ... where $\gamma = c_p/c_v$ is the ratio of the specific heats at constant pressure and constant volume ..."

9. L200. The choice of w as a symbol for the weights is unfortunate as it may lead to confusion with the vertical velocity. Please replace the symbol.

Response: Thank you for pointing out this notation conflict. We have replaced the filter-weight symbol w with $G_{j,m}$ so that it cannot be confused with the vertical velocity.

Revised manuscript text [Lines 316–321]: "In GMCORE, we apply an adaptive zonal Gaussian convolution filter for dynamical tendencies along each latitude circle ... the filtered field M_{filt} can be written ... where $G_{j,m}$ is the Gaussian weight at offset m on the j-th latitude circle, and H_j is the corresponding half-width of the stencil."

10. Equation (23). In the context of this equation, substantial information is missing to interpret its meaning. What is the purpose of W_j, i. e., in where exactly in the discretization is it being used?

Response: Thank you for asking us to clarify the role of W_j. We have added its relation to the discrete stencil. W_j is the continuous nondimensional width diagnosed from the local CFL-like constraint. It is converted to an odd stencil size N_j, with $N_j = 2H_j + 1$, so H_j is the half-width used in the actual convolution. W_j also sets the Gaussian standard deviation through the prescribed shape parameter.

Revised manuscript text [Lines 322–334]: The manuscript defines the continuous width parameter W_j from the local zonal stability constraint and then states: "The diagnosed continuous width W_j is converted to the discrete stencil size by taking the smallest odd integer not smaller than W_j, with a minimum stencil size of three grid points: $N_j = max[3, oddceil(W_j)]$. ... For a stencil of width $N_j = 2H_j + 1$ ..."

11. Figure 3->5. Are the blue dots representing the time series of the relative positions. Please indicate the trend by color-coding or labels.

Response: Thank you for asking us to clarify the meaning of the blue points. We have revised the caption to state explicitly that the blue points in the right panel are not a time series. Each point is the final NHD–NHS storm-center displacement from one paired experiment, and the labels identify the initial perturbation latitude and horizontal resolution.

Revised manuscript text [Lines 456–461]: "In the right panel, each blue dot shows the NHD–NHS difference in final storm-center position at 240 h for one independent paired experiment ... Labels indicate the initial perturbation latitude and horizontal resolution; the dots do not represent a time series. Storm centers are diagnosed directly from the grid-point minimum of surface pressure."

12. **L151.** Remove the excessive whitespace between "and" and "discretization".

Response: Thank you for identifying this spacing issue. It has been corrected in the revised manuscript.

Revised manuscript text [Lines 160–165]: The former sentence containing the spacing problem has been rewritten. The revised section now reads: "The regular latitude–longitude grid remains widely used in several established atmospheric models ... GMCORE retains this grid structure as a practical choice that is consistent with its existing numerical framework."

13. **L154.** Insert a whitespace after the sentence ending with "the planetary surface a."

Response: Thank you for identifying this missing whitespace. It has been corrected in the revised manuscript.

Revised manuscript text [Lines 189–194]: The former sentence containing the missing whitespace has been reorganized. The revised passage reads: "Let a be the reference planetary radius and r_c, r_e, and r_v the local radial distances at cell, edge, and vertex locations. A superscript (a) denotes the corresponding horizontal geometry on the reference sphere. The deep-atmosphere metric is therefore introduced directly through the local lengths and areas ..."

14. **Author contributions.** Use the appropriate past/perfect tense and replace "based" with "basic".

Response: Thank you for this suggestion. We have rewritten the Author Contributions statement using consistent present-perfect wording and corrected "based" to "basic."

Revised manuscript text [Lines 579–581]: "The deep-atmosphere extension has been developed collaboratively by the authors. LD has completed the basic nonhydrostatic framework and conceived the idea for this study. QC has implemented the deep-atmosphere extension and conducted the numerical experiments. BW has provided suggestions on model development. All authors have contributed to the writing and revision of the manuscript."

Manuscript ID: egusphere-2026-2297

Responses to Reviewer 2

We would like to thank the Reviewer for the careful reading of the manuscript and for the constructive comments and suggestions. We have revised the manuscript accordingly and provide point-by-point responses below. Our responses are shown in blue, the corresponding changes made in the revised manuscript are shown in red, and the Reviewer's comments are shown in black.

Brief Summary:

The Reviewer regards the deep-atmosphere GMCORE formulation as useful to document in the open literature and considers the presented baroclinic-wave and tropical-cyclone tests reasonable. The Reviewer also notes that the multiple tropical-cyclone initial conditions help establish that the track signal is systematic, while offering a set of mainly minor suggestions aimed at improving notation, numerical-method clarity, terminology, and presentation.

Response: Thank you very much for the careful and constructive assessment. We particularly appreciate the emphasis on clarity, because several of the points identified places where our notation or wording could give an impression different from what is actually implemented. In the revision, we have clarified the relation between the deep-atmosphere geometry and gravity, distinguished the generalized and terrain-following vertical coordinates, documented the Lorenz staggering and SWIFT/PPM treatment, clarified the temporal and vertical increments, expanded the polar-filter description, added model resolution information, and revised the relevant terminology and figure captions. Where an original statement was not sufficiently supported by the present experiments, we chose to remove or soften it rather than defend a stronger claim. We respond to each point below.

Line numbers cited below refer to the revised manuscript supplied with this response after accepting the tracked changes.

Specific points

1. Line 36. This is not strictly incorrect, but a more natural viewpoint is that the deep atmosphere equations are the more fundamental equation set and the shallow-atmosphere equations are an approximation.

Response: Thank you for this helpful suggestion. We agree that this is the more natural hierarchy of the equation sets. We have revised the sentence accordingly so that the deep-atmosphere equations are presented as the more fundamental set and the shallow-atmosphere equations as an approximation obtained by additional assumptions.

Revised manuscript text [Lines 39–47]: "The deep-atmosphere equations are generally considered to be a more fundamental set than the traditional shallow-atmosphere equations ... Standard shallow-atmosphere equations project the planetary rotation vector onto the local vertical and neglect the horizontal component ..."

2. Line 55. while most nonhydrostatic models use a height-based vertical coordinate. (Hydrostatic models commonly use a pressure- or mass-based coordinate.)

Response: Thank you for pointing this out. We have revised "most models" to "most nonhydrostatic models" as suggested.

Revised manuscript text [Lines 59–61]: "An important feature of the present formulations is that the deep-atmosphere extension is represented within the dry terrain-following mass-based coordinate while most nonhydrostatic models use height-based vertical coordinate (Wood and Staniforth, 2003)."

3. Lines 72–74. The sentence is a bit awkward because Wood and Staniforth (2003) did not use the vector-invariant form. Can it be rephrased?

Response: Thank you for noting this distinction. We have reorganized the sentence so that the source of the vector-invariant/Lamb-transformed form is separated from the deep-atmosphere formulations. Gassmann and Herzog (2008) is now cited for the vector-invariant formulation, while Wood and Staniforth (2003), Borchert et al. (2019), and Skamarock et al. (2021) are cited for the deep-atmosphere formulation and implementation context.

Revised manuscript text [Lines 77–80]: "Following the vector-invariant formulation based on the Lamb transformation (Gassmann and Herzog, 2008), together with the deep-atmosphere formulations of Wood and Staniforth (2003), Borchert et al. (2019), and Skamarock et al. (2021), GMCORE solves the fully compressible, nonhydrostatic deep-atmosphere equations in a dry terrain-following mass-based coordinate in vector-invariant form."

4. Some things are not clear about equations (1)–(7) and the subsequent discussion. Is the constant G related to g(r) in some way, or is it an arbitrary constant? Is G the same as g0 introduced later in the definition of π (equation (14))? What is s (line 124), and how does it relate to η? Is the (r/a)² factor in (2) a geometrical factor (as in (14)) rather than describing the vertical variation of g(r)?

Response: Thank you for this careful comment. The original notation did not distinguish these roles clearly enough. In the revised manuscript, g_0 denotes the reference gravitational acceleration at the planetary surface $r = a$, while the physical gravitational acceleration varies with radius as $g(r) = g_0(a/r)^2$. We also define s explicitly as the generalized vertical coordinate used in the Wood and Staniforth (2003) derivation, whereas η is the terrain-following hybrid coordinate used in the GMCORE implementation. Finally, the factor $(r/a)^2$ that appears in the deep mass-coordinate formulation is a geometrical area/Jacobian factor associated with the radial expansion of spherical control surfaces; it is distinct from the physical inverse-square variation of $g(r)$. We have revised the surrounding explanation so that these quantities are not conflated.

Revised manuscript text [Lines 80–82 and 130–149]: "Compared to the shallow-atmosphere equations, the deep extension introduces three important changes: the constant planetary radius a is replaced by the local radial distance $r = a + z$, the constant gravity g_0 becomes altitude-dependent $g(r) = g_0(a/r)^2$ ..." "They denoted s as the generalized vertical coordinate ... We use the dry mass π to substitute the generalized coordinate s and introduce terrain-following coordinate η ..." The subsequent hydrostatic relation in Eqs. (14)–(16) retains the geometrical $(r/a)^2$ factor in the mass-coordinate formulation.

5. Line 143. dictates the dry atmospheric mass?

Response: Thank you for pointing this out. We agree that "dry" should be specified here and corrected "atmospheric mass" to "dry atmospheric mass" during the revision. The relevant paragraph was subsequently removed in response to Comment 6.

Revised manuscript text [Lines 130–158]: The paragraph containing the phrase discussed in this comment is no longer present in the final revised manuscript, because that comparison paragraph was subsequently removed in response to Comment 6. The final Sect. 2.2 proceeds directly through the mass-coordinate definition, radial-distance diagnosis, and the spherical-geometry assumptions.

6. Lines 144–145. I don't understand this remark. Height-based coordinate models typically predict density, or density can easily be computed from the predicted variables. Computing the mass in an atmospheric layer is then simply a case of doing a (discrete) vertical integral, no more complicated than (17).

Response: Thank you for this correction. We agree that the original paragraph overstated the contrast with height-based coordinates. Our original wording was motivated by the possible practical convenience of a mass coordinate for some layer-integrated physical quantities, but this possible advantage has not been demonstrated by the experiments in the present manuscript. After reconsidering the point, we decided that the most careful response is to remove the paragraph rather than retain a claim that would require further dedicated evidence.

Revised manuscript text [Lines 130–158]: The original paragraph comparing the complexity of mass- and height-coordinate coupling to physical parameterizations has been removed. The final Sect. 2.2 now focuses on the definition of the mass-based coordinate, the radial-distance diagnosis, and the spherical-geometry assumptions.

7. Near line 156, perhaps mention that GMCORE uses a Lorenz vertical grid.

Response: Thank you for this suggestion. We have added the Lorenz staggering explicitly. GMCORE uses Arakawa C-grid staggering in the horizontal and Lorenz staggering in the vertical, with dry mass and thermodynamic variables on full levels and vertical velocity and vertical coordinate velocity on half levels.

Revised manuscript text [Lines 166–172]: "GMCORE uses an Arakawa C-grid staggering in the horizontal and a Lorenz staggering in the vertical ... Dry mass and thermodynamic variables are defined at the full levels ... The vertical velocity w and vertical coordinate velocity $\dot{\eta}$ are defined at the half levels."

8. Lines 158–160. Do you really use a third-order polynomial reconstruction? Bendall and Kent used the quadratic PPM reconstruction. Also, Bendall and Kent were targeting cubed-sphere grids; are there any issues in applying the scheme near the poles of a longitude-latitude grid?

Response: Thank you for pointing this out. We have corrected the reconstruction description to PPM, consistent with Bendall and Kent (2025). Regarding the application of SWIFT on the latitude–longitude grid, SWIFT mainly addresses the multidimensional inconsistency introduced by cross-directional transport, for which strict monotonicity cannot be maintained as directly as in one-dimensional transport. This improvement is made at the algorithmic level and is not closely tied to the specific grid discretization. We therefore use the same SWIFT treatment on the latitude–longitude grid.

Revised manuscript text [Lines 257–260]: "Tracer advection is handled by the SWIFT scheme (Bendall and Kent, 2025), which is derived from the FFSL formulation (Lin and Rood, 1996) with specific modifications to preserve monotonicity in two-dimensional transport and relies on PPM for the spatial reconstruction of tracers."

9. Line 178. Here I think you mean the temporal pressure increment (see equation (20)), but in equation (18) δp appears to be a vertical pressure increment. Please be explicit, or you will quickly lose readers. Also, what is gamma in equation (20)?

Response: Thank you for identifying this ambiguity. In the revised text, δ is used for the vertical increment across a model layer, whereas the temporal pressure increment is written explicitly as the difference between the updated and previous-stage pressure. We have also introduced γ as the ratio of the specific heats at constant pressure and constant volume, $\gamma = c_p/c_v$. This makes the two different types of increments explicit in the time-integration discussion.

Revised manuscript text [Lines 253–255 and 294–299]: "The symbol δ denotes the vertical increment across a model layer." "At full levels, the temporal increment of pressure $p^\tau - p^*$ is diagnostically linked to vertical increment of $\delta\varphi$ and the thermodynamic properties through the linearized equation of state ... where $\gamma = c_p/c_v$ is the ratio of the specific heats at constant pressure and constant volume ..."

10. Equations (22) and (23). How is W_j related to H_j?

Response: Thank you for asking us to clarify this relation. W_j is the continuous width parameter diagnosed from the local CFL-like constraint. It is converted to the smallest admissible odd stencil size N_j, and the actual convolution half-width is $H_j = (N_j - 1)/2$, equivalently $N_j = 2H_j + 1$.

Revised manuscript text [Lines 330–334]: "The diagnosed continuous width W_j is converted to the discrete stencil size by taking the smallest odd integer not smaller than W_j, with a minimum stencil size of three grid points: $N_j = max[3, oddceil(W_j)]$. ... For a stencil of width $N_j = 2H_j + 1$ ..."

11. Lines 217–219. How large does N_j become near the pole? The communication cost must become significant at some point as resolution is refined.

Response: Thank you for raising this practical question. At 1° horizontal resolution, the maximum half-width in the polar processes is typically about $H_j \approx 90$ grid points, corresponding to a total stencil width $N_j \approx 181$. The wider halo is not used uniformly by all processes: only the high-latitude processes require the largest width, and only the arrays to which the filter is applied use the expanded communication halo. For the resolutions considered in this manuscript, we find the additional communication and memory cost manageable. We nevertheless agree that the cost becomes increasingly important as resolution is refined; optimization of this communication pattern is ongoing, and our group is also exploring quasi-uniform/SCVT-type grid approaches for future developments.

Revised manuscript text [Lines 330–343]: "For a stencil of width $N_j = 2H_j + 1$ ... It should be noted that the wider communication halo is required only for the variables to which the filter is applied. In the parallel implementation, processes covering higher latitudes therefore use wider halos for those variables. In practice with a horizontal resolution of 1°, this half width halo usually reaches 90 points

at the two poles ... Nevertheless, the additional communication cost remains manageable for the resolutions considered here."

12. Lines 250–256. The word 'configuration' is sometimes used to distinguish the full radius and small radius cases, and sometimes to distinguish the shallow-atmosphere and deep atmosphere cases, with the potential to confuse the reader. Can you rephrase? Check also for other occurrences.

Response: Thank you for noting this ambiguity. We have revised the terminology so that the standard-Earth-radius and reduced-radius X20 cases are referred to as experiments, while NHD and NHS are used to distinguish the deep- and shallow-atmosphere equation-set configurations. We also checked the surrounding text for the same usage.

Revised manuscript text [Lines 404–410 and 445–446]: The baroclinic-wave discussion uses "standard Earth-radius experiment" and "X20 experiment" for the planetary-radius cases. The tropical-cyclone section states that the experiment is conducted with both the "nonhydrostatic deep-atmosphere (NHD) and nonhydrostatic shallow-atmosphere (NHS) configurations."

13. What resolution, horizontal and vertical, was used for the baroclinic wave test? What vertical resolution was used for the tropical cyclone test?

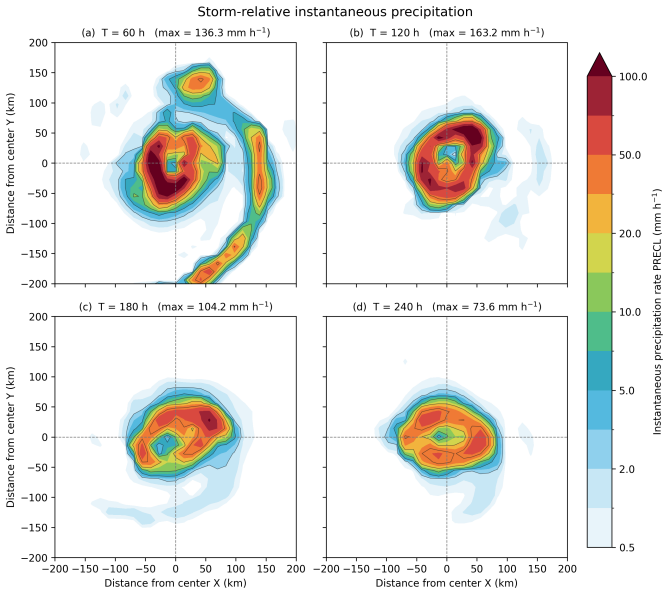
Response: Thank you for requesting these model-specific resolution details. The baroclinic-wave experiment uses a 1° (360×180) horizontal grid and the 30-level CAM vertical grid with a model top of 2.255 hPa (approximately 30 km). The tropical-cyclone experiments use 0.25° and 0.125° horizontal resolutions and the same 30-level vertical grid.

Revised manuscript text [Lines 366–368 and 439–444]: "The simulations use the 30-level vertical grid adopted from CAM, with the model top located at 2.255 hPa, corresponding to an approximate geometric height of 30 km. The horizontal resolution is 1°, corresponding to a 360×180 regular latitude–longitude grid." The tropical-cyclone section notes the "low model top (about 30 km)" and states: "We follow the standard setup of Reed and Jablonowski (2011) and run this case at a horizontal resolution of 0.25° and 0.125° for 10 days with the same vertical grid as the baroclinic-wave."

14. Figure 4 caption and line 325. The figure does not show rainfall, so the reader cannot see any spiral rainband structures.

Response: Thank you for pointing this out. We agree that the figure does not show rainfall. Because the present manuscript does not analyze the formation or mechanism of the rainbands, we decided not to add a separate rainfall figure simply to support that descriptive statement. Instead, we removed the rainband wording and restricted the discussion to the vertical-velocity structure that is actually shown in the figure.

Still, we present the spiral rainfall plot here



Revised manuscript text [Lines 473–488]: The revised Fig. 6 caption states that the mean vertical-velocity field illustrates "a core of intense upward motion centered at the origin." The corresponding

text states: “In Fig. 6a, the mean vertical velocity field exhibits a compact core of strong ascent near the storm center. This indicates that the mature vortex maintains a well-defined eyewall-like updraft region.” No spiral-rainband statement is made.

Typos etc.

Equations should be punctuated just like the rest of the text. Line 85. rate of planetary? Line 148. matches → match. Line 314. the present supplementary?

Response: Thank you for pointing out these presentation issues. We have checked the displayed equations and added punctuation according to their grammatical role in the surrounding sentences. We have also reviewed the wording describing the planetary rotation, corrected the relevant subject–verb agreement, and replaced the earlier wording with “the Supplementary Material” in the tropical-cyclone discussion.

Revised manuscript text [Lines 90–94, 147–149, and 469]: The governing-equation definitions now use the wording “Ω is the planetary angular rotation velocity”; the “matches->match” issue was removed due to content adjustment; and the tropical-cyclone discussion now states: “As already indicated in the Supplementary Material ...” Equation punctuation has also been checked throughout the revised manuscript.